Editors' Suggestion

Photonic Flywheel in a Monolithic Fiber Resonator

Kunpeng Jia,[1,2,*] Xiaohan Wang,[1,2,*] Dohyeon Kwon,[3] Jiarong Wang,[2] Eugene Tsao,[2] Huaying Liu,[1,2] Xin Ni,[1] Jian Guo,[1] Mufan Yang,[1] Xiaoshun Jiang,[1] Jungwon Kim,[3] Shi-ning Zhu,[1] Zhenda Xie,[1,†] and Shu-Wei Huang[2,‡]

[1]*National Laboratory of Solid State Microstructures, School of Electronic Science and Engineering, College of Engineering and Applied Sciences, School of Physics, and Collaborative Innovation Center of Advanced Microstructures, Nanjing University, Nanjing 210093, China*

[2]*Department of Electrical, Computer and Energy Engineering, University of Colorado Boulder, Boulder, Colorado 80309, USA*

[3]*Department of Mechanical Engineering, Korea Advanced Institute of Science and Technology, Daejeon 34141, Republic of Korea*

(Received 2 June 2020; accepted 27 August 2020; published 1 October 2020)

We demonstrate the first compact photonic flywheel with sub-fs time jitter (averaging times up to 10 μs) at the quantum-noise limit of a monolithic fiber resonator. Such quantum-limited performance is accessed through novel two-step pumping scheme for dissipative Kerr soliton generation. Controllable interaction between stimulated Brillouin lasing and Kerr nonlinearity enhances the DKS coherence and mitigates the thermal instability challenge, achieving a remarkable 22-Hz intrinsic comb linewidth and an unprecedented phase noise of -180 dBc/Hz at 945-MHz carrier at free running. The scheme can be generalized to various device platforms for field-deployable precision metrology.

DOI: 10.1103/PhysRevLett.125.143902

Dissipative Kerr soliton (DKS) frequency comb [1,2], generated by pumping a high-Q monolithic resonator with a resonant continuous-wave (cw) single-mode laser, has recently emerged as a promising complement to the traditional mode-locked laser frequency comb [3–6]. Access to considerably larger comb spacings in nonconventional spectral ranges has led to continued enthusiasm since its advent. Demonstrations of photonic frequency synthesizer [7,8], microphotonic astrocomb [9,10], dual-comb spectroscopy [11,12], and coherent optical communication [13,14] revealed the unique performance of DKS frequency comb, and reassured further expansion of already remarkable applications. However, despite the massive achievements in the spectral domain, noise analysis of DKS in the time domain is still lacking and thus it remains questionable whether DKS can also serve as an optical flywheel [5], where the pristine temporal periodicity with sub-optical-cycle timing jitters can be utilized for intriguing applications at the intersection of ultrafast optics and microwave electronics, including photonic analog-to-digital converters (ADCs) for next-generation radar and communication systems [15–17], coherent waveform synthesizers for pushing the frontiers of femtosecond and attosecond science [18–20], ultralow-noise microwave signals generation [21–25], and timing distribution links for synchronizing large-scale scientific facilities like x-ray free-electron lasers and the extreme light infrastructure [26–32].

On-chip monolithic resonators feature strong mode confinement and large Kerr nonlinearity that fundamentally elevate the quantum-limited phase noise and prohibit us from achieving timing jitter at the optical flywheel level [2,33]. Moreover, sophisticated pump noise control and thermal effect management are required to practically achieve the quantum-limited phase noise. As pump is an integral part of the DKS frequency comb [1], narrow-linewidth pump is necessary for reducing the pump-to-comb noise conversion to reach the quantum-limited comb coherence [34]. Mitigation of the strong thermal nonlinearity is also a fundamental challenge for stable DKS generation. Traditionally, either active precision control of pump and resonators is implemented to reduce the thermal effect [35,36] or an auxiliary laser is included to compensate for the pump induced thermal dynamics [37,38]. Both mitigation schemes inevitably add system complexity and compromise the advantages of the DKS frequency comb as an integrated device.

In this work, we demonstrate for the first time a compact photonic flywheel based on DKS generation in a relatively unexplored platform of monolithic fiber Fabry-Perot (FFP) resonator [39–41]. Our theoretical noise analysis suggests that FFP resonator is a promising photonic flywheel platform where subfemtosecond and even 100-attosecond timing jitters can be achieved at gigahertz repetition rate. To mitigate challenges in DKS generation and reach the quantum-limited performance, we devise a novel two-step pumping scheme where the DKS is formed from a secondary pump generated in the same FFP resonator through the cross-polarized stimulated Brillouin lasing (SBL). Advantages of such two-step pumping scheme are twofold. First, resonator SBL exhibits an orders-of-magnitude linewidth reduction [42,43] and thus as the secondary pump, it

has a much higher spectral purity in comparison to the primary laser, reducing the pump-to-comb noise conversion [34] and relaxing the laser linewidth requirement to achieve a DKS with quantum-limited phase noise and timing jitter. Second, the primary laser and the SBL work together to compensate the detrimental cavity thermal nonlinearity that limits the reliability and robustness of DKS generation [2]. Only one cw single-mode laser is required in our two -step pumping scheme, where the primary laser evolves to effectively become an auxiliary laser while the cross-polarized SBL grows to generate DKS in the FFP resonator, resulting in a novel self-stabilized strategy for thermal management and robust DKS generation. All in all, our free-running quantum-limited DKS frequency comb achieves an unprecedented intrinsic linewidth of 22 Hz, characterized by a short delay self-heterodyne interferometry (SDSHI) [44], and breaks for the first time into the attosecond integrated timing jitter realm of 995 attosecond for averaging times up to 10 μs, measured with an all-fiber reference-free Michelson interferometer (ARMI) timing jitter measurement apparatus [45].

Our FFP resonator [inset of Fig. 1(a)] is fabricated from a commercially available highly nonlinear fiber (HNLF, NL-1550-POS, YOFC) with nonlinear coefficient over 10 $W^{-1}\,km^{-1}$ and attenuation below 1.5 dB/km. The 105-mm long cavity length results in a free spectral range (FSR) of 945.4 MHz as shown in Fig. 1(b). Both fiber ends are mounted in ceramic ferrules, finely polished, and then coated with ten-layer pairs of Ta_2O_5 and SiO_2 using the ion assisted deposition method. Such a Bragg mirror achieves a reflectivity of over 99.6% from 1530 to 1570 nm. Of note, gigahertz comb spacing is especially suitable for applications like dual-comb spectroscopy and photonic ADCs [46,47]. With a negligible propagation loss of

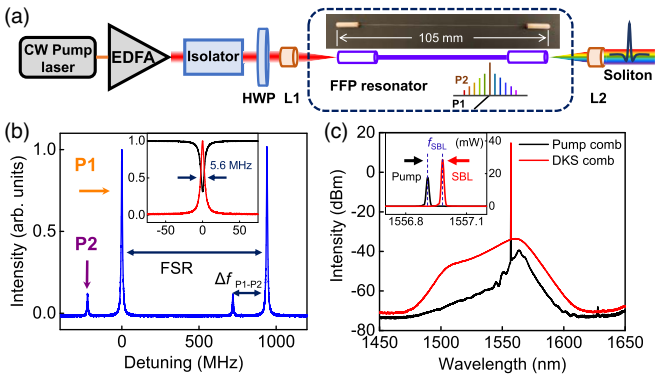

FIG. 1. (a) Experimental setup for self-stabilized DKS generation. $L1$ and $L2$: aspheric lens. Inset: picture of the FFP resonator. (b) Cold-cavity transmission spectrum around 1557 nm. Inset: Enlarged view of the transmission and reflection signals across the $P1$ resonance. (c) When the primary laser is polarized along $P1$, efficient SBL generation (inset) followed by DKS frequency comb generation, both polarized along $P2$, is observed and measured.

HNLF, the quality factor (Q) of the FFP resonator is mainly defined by the dielectric mirror coatings at the two ends. Thus, its Q and the comb generating pump power both scale favorably at lower comb spacings, which is critically different from on-chip monolithic resonators with propagation-limited Q. The FFP resonator resonance linewidth is measured and fitted to be 5.6 MHz, corresponding to a Q of 3.4×10^7 [inset of Fig. 1(b)]. Group velocity dispersion of -3 fs^2/mm at 1557 nm is characterized with the spectral interferometric method [48]. Similar monolithic FFP resonators have been previously utilized for Brillouin-enhanced hyperparametric frequency comb generation [39] and synchronously pulse pumped DKS generation [40]. However, our work presents the first demonstration of cw pumped DKS generation in a monolithic FFP resonator, which is the key to the photonic flywheel demonstration.

In an FFP resonator, there are two families of cavity modes with orthogonal polarizations ($P1$ and $P2$) due to the stress-induced birefringence [Fig. 1(b)] [49]. The offset frequency $\Delta f_{P1\text{-}P2}$ between these two sets of resonances can be finely controlled by applying a different level of stress on the FFP resonator [50]. For the DKS generation, a tunable external cavity diode laser followed by an erbium-doped fiber amplifier (EDFA) is coupled into the FFP resonator as the primary laser [Fig. 1(a)]. When the primary laser is polarized along $P1$ with over 0.19 W power, SBL generation can be observed at the frequency downshifted from the primary laser by $f_{SBL} = 9.242$ GHz. As we further increase the primary laser power to 4.3 W, the SBL will be efficient enough that it eventually overtakes the primary laser and becomes the dominant comb generating secondary pump in the resonator [inset of Fig. 1(c)]. At this time, the intracavity power of the SBL will be 3 dB higher than that of the primary laser. Careful analysis of SBL and cavity mode structure reveals that the first-order Stokes Brillouin gain spectrum overlaps with the $P2$ resonance on the red-detuned side when the offset frequency $\Delta f_{P1\text{-}P2}$ is set to be 224 MHz. Thus, we can locate the SBL at the red-detuned side of the $P2$ resonance while the primary laser is still at the blue-detuned side of the $P1$ resonance [50]. As elaborated later in Fig. 2, such novel two-step pumping arrangement results in a self-stabilized strategy for thermal management and robust DKS generation. Of note, the choice for pump mode of $P1$ and $P2$ is arbitrary as long as the Brillouin shift frequency matches with the offset frequency of the corresponding cross-polarized cavity resonances by stress tuning. Importantly, the cascaded SBL is strictly forbidden in this cross-polarization arrangement as only the first-order Stokes Brillouin gain spectrum can ever overlap with the cavity resonance [50]. This is in stark contrast to the previous literature [39] where the cascaded SBL interacts with the cavity Kerr nonlinearity to enhance the hyperparametric oscillation but interrupt the DKS generation [54,55].

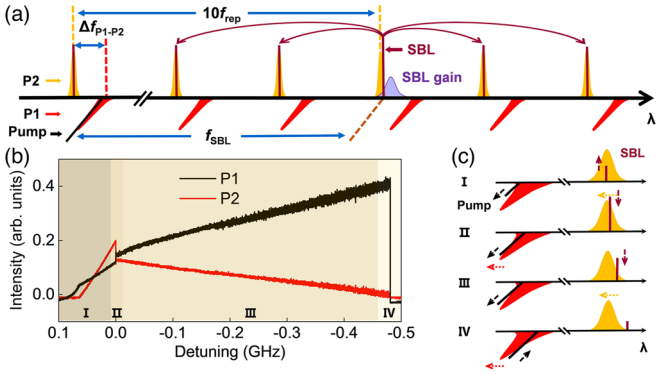

FIG. 2. (a) Schematic of the self-stabilized DKS generation. When the DKS is generated, the $P1$-polarized primary laser remains on the blue-detuned side while the $P2$-polarized SBL secondary pump is pushed to the red-detuned side of the cavity resonances. Such arrangement mitigates the thermal instability and facilitates robust DKS generation. (b) Cavity transmission at both polarizations during the primary laser scan from higher to lower frequencies over a resonance. (c) Principle of the self-stabilized strategy for thermal management and robust DKS generation. Stage I: SBL growth; stage II: DKS generation; stage III: chaotic oscillation; and stage IV: trivial off-resonance state.

Our configuration suppresses these unnecessary nonlinear interactions and promotes the generation of low-noise DKS.

When we further tune the $P1$-polarized primary laser into the resonance from the blue-detuned side, a $P2$-polarized DKS frequency comb centered around the SBL is obtained [DKS comb in Fig. 1(c)]. Its 3-dB and 30-dB bandwidths are about 20 and 115 nm, respectively. The power of generated DKS comb is about 98 μW (corresponding to 0.1 pJ pulse energy) with conversion efficiency of 2.3×10^{-5} from the primary laser. Following the development of the DKS frequency comb, we also observe a 10-dB weaker $P1$-polarized comb [pump comb in Fig. 1(c)] that is generated through cross-phase modulation (XPM) of the DKS [56]. The DKS is self-stabilized and it stays over hours without any active control. The DKS state is deterministic in that it can be repeatedly and reliably generated following the same pump tuning protocol. To elucidate the efficacy of the two-pumping scheme, we record the cavity transmission at both polarizations simultaneously while the primary laser frequency is scanned at a speed of 1.84 GHz/s across the $P1$ resonance from the blue-detuned side [Fig. 2(b)]. The principle of the self-stabilized strategy for thermal management and robust DKS generation are illustrated in Fig. 2(c). When the primary laser is first tuned closer to the $P1$ resonance, the intracavity power gradually increases to above the cross-polarized SBL threshold for the initial SBL growth around the peak of the $P2$ resonance (stage I). When the primary laser is further tuned into the $P1$ resonance, the SBL secondary pump is pushed across the $P2$ resonance to the red-detuned side following the shift of the Brillouin gain peak (stage II). Of note, the SBL secondary pump experiences a much slower detuning speed with a slow-down factor of 15 compared to that of the primary laser, considering 5.6-MHz cavity resonance linewidth and 79-MHz Brillouin gain bandwidth [39,57]. At the end of stage II, discrete transmission steps characteristic of DKS generation are observed. In general, such an intracavity power drop leads to cavity cooling and consequently resonance blueshift that induces thermal instability [37,38,58]. In contrast, here the dynamics is very different as the primary laser is still on the blue-detuned side of the resonance. The resonance blueshift now leads to an increased cavity loading from the primary laser and it compensates for the intracavity power drop from the SBL secondary pump alone. Thus, thermal equilibrium is still maintained at the DKS state. Such self-stabilized strategy mitigates the thermal instability and facilitates robust DKS generation. At stage III, the primary laser continues to get closer to the $P1$ cavity resonance while the SBL secondary pump is pushed further away from the $P2$ cavity resonance, resulting in the monotonic increase and decrease of the $P1$ and $P2$ transmission signals, respectively. Finally, the

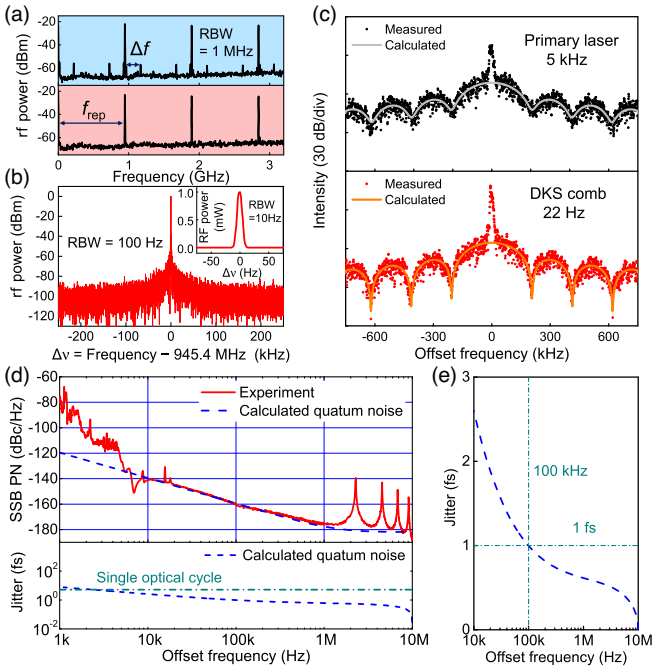

FIG. 3. (a) rf beat notes of the mixed polarization output (top panel) and the $P2$-polarized DKS frequency comb (bottom panel). (b) Fundamental beat note of the DKS frequency comb on logarithmic scale and linear scale (inset). (c) SDSHI results of the primary laser and the DKS frequency comb, showing a significant linewidth narrowing from 5 kHz to 22 Hz. (d) Top panel: single sideband phase noise of DKS frequency comb scaled at 1-FSR carrier (red solid curve), reaching the quantum-noise limit (blue dashed curve) for offset frequencies above 10 kHz. Bottom panel: sub-optical-cycle integrated timing jitter. (e) Enlarged view of the integrated timing jitter, showing a subfemtosecond jitter for averaging times up to 10 μs.

primary laser is also scanned to the red-detuned side of the $P1$ resonance, resulting in a trivial thermal instability that quickly pushes the system off the resonance (stage IV).

Figure 3(a) plots the radio frequency (rf) spectra of the beat notes from the mixed polarization output (top panel) and the $P2$-polarized DKS (bottom panel). Clean rf beat notes with signal-to-noise ratio (SNR) greater than 45 dB at 1-MHz resolution bandwidth (RBW) are observed at harmonic frequencies. The frequency separation Δf between each harmonic beat note and its nearest side peaks is measured to be 224 MHz, in a good agreement with the offset frequency $\Delta f_{P1\text{-}P2}$ between orthogonal modes in the FFP resonator. The rf measurement further shows that the two orthogonally polarized combs are synchronized with the same repetition frequency and the same narrow linewidth [50] within the instrument limit, which can be explained by the XPM coupling in between. Importantly, $P2$-polarized DKS frequency comb can be well isolated and selected by a combination of a half-wave plate (HWP) and a polarizing beam splitter (PBS) cube at the output. Figure 3(b) is the enlarged view of its fundamental beat note, showing a resolution-limited linewidth of 10 Hz.

Our two-step pumping scheme not only mitigates the thermal instability challenge, but also provides a passive linewidth narrowing for the secondary pump through the cavity-enhanced SBL process. It relaxes the laser linewidth requirement for the DKS to reach the quantum-limited phase noise and timing jitter. In this process, the SBL (or the secondary pump) has a much higher spectral purity than its pump (or the primary laser) with a linewidth narrowing factor of $(1+\gamma_S/\Gamma)^2$ where Γ and γ_S are the cavity linewidth and the Brillouin gain bandwidth, respectively [39]. In our FFP resonator where $\Gamma = 5.6$ MHz and $\gamma_S = 79$ MHz, a narrowing factor of 228 is expected such that the secondary pump linewidth can be reduced to 22 Hz from the 5-kHz primary laser. Experimentally, we build an SDSHI to characterize such significant linewidth narrowing. SDSHI uses short delay fibers and curve fitting of the measured coherent envelope to suppress the $1/f$ Gaussian noise and obtain a more accurate estimate of the intrinsic laser Lorentzian linewidth [44,50]. Figure 3(c) plots the SDSHI experimentally measured results overlaid with theoretically calculated results of the primary laser (top panel) and the DKS frequency comb (bottom panel). A good agreement between the measurement and the calculation is obtained, and it confirms the linewidth narrowing capability of our two-step pumping scheme. Consequently, our DKS frequency comb has an unprecedented 22-Hz intrinsic linewidth that facilitates the achievement of quantum-limited phase noise and timing jitter into the attosecond realm.

The phase noise and timing jitter are analyzed with the ARMI timing jitter measurement method [50], which provides attosecond timing jitter precision with a -194 dBc/Hz measurement noise floor at 1-GHz carrier (equivalent to 2×10^{-3} as^2/Hz) [45]. For our FFP resonator, the quantum-limited phase noise should have a characteristic 20 dB/decade roll-off and approach a white noise floor of -182 dBc/Hz with a corner offset frequency of 1 MHz [33]. Such low phase noise floor cannot be accurately assessed by direct photodetection methods that are typically shot noise limited at -160 dBc/Hz level [45,59,60]. Figure 3(d) plots the experimentally measured single sideband phase noise (SSB PN) spectrum overlaid with the theoretically calculated quantum limit. Excellent agreement between the measurement and the theory is obtained for offset frequencies above 10 kHz, except for a few high-frequency measurement artifact spikes resulting from the 45-m-long fiber link in the ARMI setup [45]. The integrated timing jitter is 2.5 fs for averaging times up to 100 μs, corresponding to less than half of the optical cycle at the DKS center wavelength. It further breaks into the attosecond timing jitter realm of 995 attosecond for averaging times up to 10 μs [Fig. 3(e)]. For offset frequencies below 10 kHz, relative intensity noise (RIN) from the EDFA induced excessive noise through self-steepening dominates the SSB PN spectrum. It rapidly increases the integrated timing jitter to above the single-optical-cycle level for averaging times up to 1 ms. However, these low frequency noise components can be well suppressed by either passively isolating the DKS setup from the environment or actively controlling the DKS power through standard electronics. Here, we choose 10-MHz Fourier frequency as the upper limit for the timing integration as the white noise floor above 10 MHz can also be significantly reduced by orders of magnitude through applying a narrowband rf filter to replace the shot noise with thermal noise [61]. The measurement confirms the demonstrated DKS frequency comb, with the novel FFP resonator platform and two-step pumping scheme, achieves an unprecedentedly low timing jitter in comparison to other on-chip combs and complements the traditional mode-locked laser frequency comb as a compact photonic flywheel.

Finally, the DKS pulse structure is characterized using a second-harmonic generation frequency-resolved optical gating (SHG FROG) system. A stable bright single-soliton pulse train with a repetition period of 1.06 ns is observed on the oscilloscope [50]. Before the pulse is directed to the SHG FROG system, it passes through a free-space grating filter and is then coupled into fiber with a coupling efficiency of 24%, to have the primary laser and secondary pump blocked. Then a dispersion compensated EDFA is used to amplify the pulse energy to 740 pJ with spectrum shown in the inset of Fig. 4(b). The pulse shape and temporal phase are retrieved using an iterative genetic algorithm [50,62] as plotted in Fig. 4(a), showing a nearly transform-limited pulse duration of 220 fs with a FROG error of 0.6%. The pulse has enough peak power for high-quality supercontinuum generation in a 6-m long dispersion-flattened HNLF (HNDS1626BA, SUMITOMO

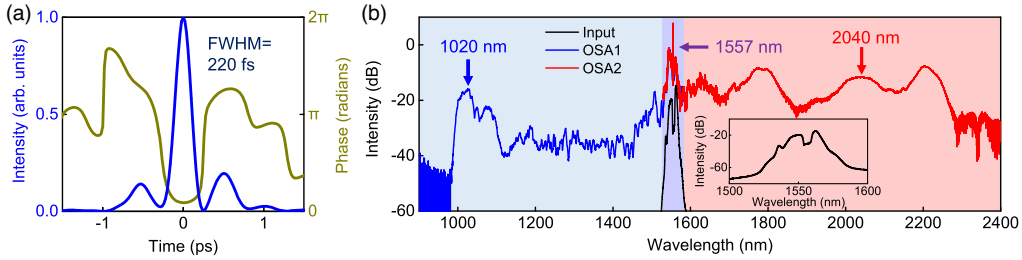

FIG. 4. (a) FROG-retrieved pulse shape and temporal phase. (b) Supercontinuum spanning more than an octave. Inset: spectrum of the amplified single-soliton pulse.

ELECTRIC) with dispersion of 5.8 ps/nm/km and dispersion slope of 0.026 ps/nm^2/km at 1550 nm. The HNLF has a high nonlinear coefficient of 24 W^{-1} km^{-1}, and its zero-dispersion wavelength is extended to 1395 nm, facilitating the generation of Cherenkov radiation at shorter wavelengths around 1 μm. Overall, the supercontinuum spans over an octave [Fig. 4(b)], where 292-pJ pulse energy is concentrated within the 2000–2300-nm range to generate a f-2f beating signal with enough signal-to-noise ratio. This signal can be fed back to the pump laser frequency through its piezo stage or the diode current, for future SHG frequency comb self-referencing [3].

In summary, we demonstrate for the first time a compact DKS photonic flywheel. The choice of FFP resonator platform enables quantum-limited subfemtosecond timing jitter at gigahertz repetition rate, and the innovation of two-step pumping scheme is instrumental in mitigating the DKS thermal instability and enforcing the DKS generation at the quantum limit. Free running, our DKS photonic flywheel achieves an intrinsic comb linewidth of 22 Hz and enters into the attosecond timing jitter realm of 995 attosecond for averaging times up to 10 μs. It has the benefit of DKS for considerably larger comb spacings in nonconventional spectral ranges but can achieve a performance that was only attainable previously in traditional mode-locked lasers. The spectrum centered at 1557 nm has a 3-dB bandwidth of 20 nm, and it can be further broadened via supercontinuum generation in dispersion-flattened HNLF to cover more than an octave. It establishes the basis for frequency comb self-referencing toward even lower time jitter at all timescales. Broader comb spectra as well as shorter pulse duration can be expected for further fiber dispersion engineering. And the fabrication methods can be improved to achieve higher finesses and lower the pump power requirement. Finally, the intrinsic compatibility between our FFP resonator platform and the existing fiber laser technology will facilitate hermetic all-in-fiber packaging to achieve the long-sought-after goal of a field-deployable precision metrology device in both spectral and time domains.

We thank Professor K. J. Vahala, Professor S. A. Diddams, Dr. I. R. Coddington, and Professor A. L. Gaeta for discussions. K. J., X. W., H. L., X. N., J. G., Z. X., and S. Z. acknowledge the support by The National Key Research and Development Program of China (2019YFA0705000, 2017YFA0303700), Key R&D Program of Guangdong Province (2018B030329001), Leading-edge technology Program of Jiangsu Natural Science Foundation (BK20192001), National Natural Science Foundation of China (51890861, 11690031, 11621091, 11674169). K. J., X. W., D. K., J. W., E. T., H. L., and S.-W. H. acknowledge the support from the University of Colorado Boulder. K. J., X. W., and H. L. acknowledge the support by China Scholarship Council (CSC). J. K. and D. K. acknowledge the support by Institute of Information & Communications Technology Planning & Evaluation (IITP) of Korea (2019-0-01349) and National Research Foundation of Korea (2018R1A2B3001793).

*These authors contributed equally to this work.
†xiezhenda@nju.edu.cn
‡ShuWei.Huang@colorado.edu

[1] T. J. Kippenberg, A. L. Gaeta, M. Lipson, and M. L. Gorodetsky, Dissipative Kerr solitons in optical microresonators, Science **361**, eaan8083 (2018).
[2] A. L. Gaeta, M. Lipson, and T. J. Kippenberg, Photonic-chip-based frequency combs, Nat. Photonics **13**, 158 (2019).
[3] J. Ye and S. T. Cundiff, *Femtosecond Optical Frequency Comb: Principle, Operation and Applications* (Springer, New York, 2005).
[4] T. Udem, R. Holzwarth, and T. W. Hänsch, Optical frequency metrology, Nature (London) **416**, 233 (2002).
[5] A. J. Benedick, J. G. Fujimoto, and F. X. Kärtner, Optical flywheels with attosecond jitter, Nat. Photonics **6**, 97 (2012).
[6] S. A. Diddams, D. J. Jones, J. Ye, S. T. Cundiff, J. L. Hall, J. K. Ranka, R. S. Windeler, R. Holzwarth, T. Udem, and T. W. Hänsch, Direct Link between Microwave and Optical Frequencies with a 300 THz Femtosecond Laser Comb, Phys. Rev. Lett. **84**, 5102 (2000).
[7] S.-W. Huang, J. Yang, M. Yu, B. H. McGuyer, D.-L. Kwong, T. Zelevinsky, and C. W. Wong, A broadband chip-scale optical frequency synthesizer at 2.7×10^{-16} relative uncertainty, Sci. Adv. **2**, 4 (2016).

[8] D. T. Spencer *et al.*, An optical-frequency synthesizer using integrated photonics, Nature (London) **557**, 81 (2018).
[9] M.-G. Suh *et al.*, Searching for exoplanets using a microresonator astrocomb, Nat. Photonics **13**, 25 (2019).
[10] E. Obrzud *et al.*, A microphotonic astrocomb, Nat. Photonics **13**, 31 (2019).
[11] M.-G. Suh, Q.-F. Yang, K. Y. Yang, X. Yi, and K. J. Vahala, Microresonator soliton dual-comb spectroscopy, Science **354**, 600 (2016).
[12] M. Yu, Y. Okawachi, A. G. Griffith, N. Picqué, M. Lipson, and A. L. Gaeta, Silicon-chip-based mid-infrared dual-comb spectroscopy, Nat. Commun. **9**, 1869 (2018).
[13] J. Pfeifle *et al.*, Coherent terabit communications with microresonator Kerr frequency combs, Nat. Photonics **8**, 375 (2014).
[14] P. Marin-Palomo *et al.*, Microresonator-based solitons for massively parallel coherent optical communications, Nature (London) **546**, 274 (2017).
[15] P. Ghelfi *et al.*, A fully photonics-based coherent radar system, Nature (London) **507**, 341 (2014).
[16] A. Khilo *et al.*, Photonic ADC: Overcoming the bottleneck of electronic jitter, Opt. Express **20**, 4454 (2012).
[17] A. Mahjoubfar, D. V. Churkin, S. Barland, N. Broderick, S. K. Turitsyn, and B. Jalali, Time stretch and its applications, Nat. Photonics **11**, 341 (2017).
[18] S.-W. Huang *et al.*, High-energy pulse synthesis with sub-cycle waveform control for strong-field physics, Nat. Photonics **5**, 475 (2011).
[19] C. Manzoni, O. D. Mücke, G. Cirmi, S. Fang, J. Moses, S.-W. Huang, K.-H. Hong, G. Cerullo, and F. X. Kärtner, Coherent pulse synthesis: Towards sub-cycle optical waveforms, Laser Photonics Rev. **9**, 129 (2015).
[20] P. Krogen, H. Suchowski, H. Liang, N. Flemens, K.-H. Hong, F. X. Kärtner, and J. Moses, Generation and multi-octave shaping of mid-infrared intense single-cycle pulses, Nat. Photonics **11**, 222 (2017).
[21] M. Endo, T. D. Shoji, and T. R. Schibli, Ultralow noise optical frequency combs, IEEE J. Sel. Top. Quantum Electron. **24**, 1 (2018).
[22] K. Jung and J. Kim, Subfemtosecond synchronization of microwave oscillators with mode-locked Er-fiber lasers, Opt. Lett. **37**, 2958 (2012).
[23] T. M. Fortier *et al.*, Optically referenced broadband electronic synthesizer with 15 digits of resolution, Laser Photonics Rev. **10**, 780 (2016).
[24] X. Xie *et al.*, Photonic microwave signals with zeptosecond-level absolute timing noise, Nat. Photonics **11**, 44 (2017).
[25] W. Weng, E. Lucas, G. Lihachev, V. E. Lobanov, H. Guo, M. L. Gorodetsky, and T. J. Kippenberg, Spectral Purification of Microwave Signals with Disciplined Dissipative Kerr Solitons, Phys. Rev. Lett. **122**, 013902 (2019).
[26] M. Xin, K. Şafak, M. Y. Peng, A. Kalaydzhyan, W.-T. Wang, O. D. Mücke, and F. X. Kärtner, Attosecond precision multi-kilometer laser-microwave network, Light Sci. Appl. **6**, e16187 (2017).
[27] X. Chen, Y. Cui, X. Lu, C. Ci, X. Zhang, B. Liu, H. Wu, T. Tang, K. Shi, and Z. Zhang, High-precision multi-node clock network distribution, Rev. Sci. Instrum. **88**, 103103 (2017).
[28] M. Xin, K. Şafak, and F. X. Kärtner, Ultra-precise timing and synchronization for large-scale scientific instruments, Optica **5**, 1564 (2018).
[29] D. Herman *et al.*, Femtosecond Timekeeping: Slip-Free Clockwork for Optical Timescales, Phys. Rev. Applied **9**, 044002 (2018).
[30] H. Hachisu, F. Nakagawa, Y. Hanado, and T. Ido, Months-long real-time generation of a time scale based on an optical clock, Sci. Rep. **8**, 4243 (2018).
[31] C. Grebing, A. Al-Masoudi, S. Dörscher, S. Häfner, V. Gerginov, S. Weyers, B. Lipphardt, F. Riehle, U. Sterr, and C. Lisdat, Realization of a timescale with an accurate optical lattice clock, Optica **3**, 563 (2016).
[32] L. C. Sinclair, H. Bergeron, W. C. Swann, E. Baumann, J.-D. Deschênes, and N. R. Newbury, Comparing Optical Oscillators across the Air to Milliradians in Phase and 10^{-17} in Frequency, Phys. Rev. Lett. **120**, 050801 (2018).
[33] A. B. Matsko and L. Maleki, On timing jitter of mode locked Kerr frequency combs, Opt. Express **21**, 28862 (2013).
[34] A. B. Matsko and L. Maleki, Noise conversion in Kerr comb rf photonic oscillators, J. Opt. Soc. Am. B **32**, 232 (2015).
[35] P. Del'Haye, K. Beha, S. B. Papp, and S. A. Diddams, Self-Injection Locking and Phase-Locked States in Microresonator-Based Optical Frequency Combs, Phys. Rev. Lett. **112**, 043905 (2014).
[36] X. Yi, Q.-F. Yang, K. Y. Yang, and K. Vahala, Active capture and stabilization of temporal solitons in microresonators, Opt. Lett. **41**, 2037 (2016).
[37] H. Zhou, Y. Geng, W. Cui, S.-W. Huang, Q. Zhou, K. Qiu, and C. W. Wong, Soliton bursts and deterministic dissipative Kerr soliton generation in auxiliary-assisted microcavities, Light Sci. Appl. **8**, 50 (2019).
[38] S. Zhang, J. M. Silver, L. D. Bino, F. Copie, M. T. M. Woodley, G. N. Ghalanos, A. Ø. Svela, N. Moroney, and P. Del'Haye, Sub-milliwatt-level microresonator solitons with extended access range using an auxiliary laser, Optica **6**, 206 (2019).
[39] D. Braje, L. Hollberg, and S. Diddams, Brillouin-Enhanced Hyperparametric Generation of an Optical Frequency Comb in a Monolithic Highly Nonlinear Fiber Cavity Pumped by a cw Laser, Phys. Rev. Lett. **102**, 193902 (2009).
[40] E. Obrzud, S. Lecomte, and T. Herr, Temporal solitons in microresonators driven by optical pulses, Nat. Photonics **11**, 600 (2017).
[41] V. Brasch, E. Obrzud, S. Lecomte, and T. Herr, Nonlinear filtering of an optical pulse train using dissipative Kerr solitons, Optica **6**, 1386 (2019).
[42] I. S. Grudinin, A. B. Matsko, and L. Maleki, Brillouin Lasing with a CaF_2 Whispering Gallery Mode Resonator, Phys. Rev. Lett. **102**, 043902 (2009).
[43] W. Loh, A. A. S. Green, F. N. Baynes, D. C. Cole, F. J. Quinlan, H. Lee, K. J. Vahala, S. B. Papp, and S. A. Diddams, Dual-microcavity narrow-linewidth Brillouin laser, Optica **2**, 225 (2015).
[44] S. Huang, T. Zhu, M. Liu, and W. Huang, Precise measurement of ultra-narrow laser linewidths using the strong coherent envelope, Sci. Rep. **7**, 41988 (2017).
[45] D. Kwon, C.-G. Jeon, J. Shin, M.-S. Heo, S. E. Park, Y. Song, and J. Kim, Reference-free, high-resolution

measurement method of timing jitter spectra of optical frequency combs, Sci. Rep. **7**, 40917 (2017).

[46] M.-G. Suh and K. Vahala, Gigahertz-repetition-rate soliton microcombs, Optica **5**, 65 (2018).

[47] D. M. B. Lesko, A. J. Lind, N. Hoghooghi, A. Kowligy, H. Timmers, P. Sekhar, B. Rudin, F. Emaury, G. B. Rieker, and S. A. Diddams, Fully phase-stabilized 1 GHz turnkey frequency comb at 1.56 μm OSA Continuum **3**, 2070 (2020).

[48] J. Y. Lee and D. Y. Kim, Versatile chromatic dispersion measurement of a single mode fiber using spectral white light interferometry, Opt. Express **14**, 11608 (2006).

[49] R. Gafsi and M. A. El-Sherif, Analysis of induced-birefringence effects on fiber Bragg gratings, Opt. Fiber Technol. **6**, 299 (2000).

[50] See Supplemental Material at http://link.aps.org/supplemental/10.1103/PhysRevLett.125.143902 for details on the experimental soliton generation and analyzation, which includes Refs. [51–53]

[51] B. Fischer, B. Hopf, M. Lindner, A. W. Koch, and J. Roths, Verification of a three dimensional FEM model for FBGs in PANDA fibers by transversal load experiments, in *Proc. SPIE 10323, 25th International Conference on Optical Fiber Sensors* 1–4 (Jeju, 2017), 103232B, https://doi.org/10.1117/12.2263262.

[52] L. R. Brovelli and U. Keller, Simple analytical expressions for the reflectivity and the penetration depth of a Bragg mirror between arbitrary media, Opt. Commun. **116**, 343 (1995).

[53] H. Bao *et al.*, Laser cavity-soliton microcombs, Nat. Photonics **13**, 384 (2019).

[54] K. I. Hagiuda, T. Hirooka, M. Nakazawa, S. Arahira, and Y. Ogawa, 40-GHz, 100-fs stimulated-Brillouin-scattering-free pulse generation by combining a mode-locked laser diode and a dispersion-decreasing fiber, Opt. Lett. **30**, 670 (2005).

[55] T. Hirooka, S. Ono, K. I. Hagiuda, and M. Nakazawa, Stimulated Brillouin scattering in dispersion-decreasing fiber with ultrahigh-speed femtosecond soliton pulse compression, Opt. Lett. **30**, 364 (2005).

[56] C. Bao *et al.*, Orthogonally polarized frequency comb generation from a Kerr comb via cross-phase modulation, Opt. Lett. **44**, 1472 (2019).

[57] J. Li, H. Lee, T. Chen, and K. J. Vahala, Characterization of a high coherence, Brillouin microcavity laser on silicon, Opt. Express **20**, 20170 (2012).

[58] Q. Li, T. C. Briles, D. A. Westly, T. E. Drake, J. R. Stone, B. R. Ilic, S. A. Diddams, S. B. Papp, and K. Srinivasan, Stably accessing octave-spanning microresonator frequency combs in the soliton regime, Optica **4**, 193 (2017).

[59] S.-W. Huang, J. Yang, J. Lim, H. Zhou, M. Yu, D.-L. Kwong, and C. W. Wong, A low-phase-noise 18 GHz Kerr frequency microcomb phase-locked over 65 THz, Sci. Rep. **5**, 13355 (2015).

[60] J. R. Stone, T. Briles, T. E. Drake, D. T. Spencer, D. R. Carlson, S. A. Diddams, and S. B. Papp, Thermal and Nonlinear Dissipative-Soliton Dynamics in Kerr-Microresonator Frequency Combs, Phys. Rev. Lett. **121**, 063902 (2018).

[61] W. Liang, D. Eliyahu, V. S. Ilchenko, A. A. Savchenkov, A. B. Matsko, D. Seidel, and L. Maleki, High spectral purity Kerr frequency comb radio frequency photonic oscillator, Nat. Commun. **6**, 7957 (2015).

[62] S.-W. Huang, H. Zhou, J. Yang, J. F. McMillan, A. Matsko, M. Yu, D.-L. Kwong, L. Maleki, and C. W. Wong, Mode-Locked Ultrashort Pulse Generation from On-Chip Normal Dispersion Microresonators, Phys. Rev. Lett. **114**, 053901 (2015).